Metallogr. Microstruct. Anal. (2013) 2:196–201
DOI 10.1007/s13632-013-0077-5

FEATURE

Best Paper in *Journal of Thermal Spray Technology:* 3D Analysis in Microstructure of Thermal Spray Coatings

The *Journal of Thermal Spray Technology* recently announced its 2012 Best Paper Award. The winning article, "Three-Dimensional Simulation of Porosity in Plasma-Sprayed Alumina Using Microtomography and Electrochemical Impedance Spectrometry for Finite Element Modeling of Properties," by O. Amsellem, F. Borit, D. Jeulin, V. Guipont, M. Jeandin, E. Boller, and F. Pauchet, was published in the March 2012 issue of JTST. The article focuses on three-dimensional analysis in microstructures of thermal spray coatings by utilizing microtomography and microstructure simulation tools.

The judges for the Best Paper Award hailed this manuscript as a "brilliant exposition of the significance and importance of microtomography in understanding the behavior of thermally sprayed coatings," and a "very forward thinking approach in thermal spray." Given the focus on microstructure and analysis of this specific manuscript, and of the importance of thermal spray technology in general, highlights of the winning article are presented here to the readers of MMA. To access the full-length article, visit the website of the *Journal of Thermal Spray Technology* at http://link.springer.com/journal/11666.

Selections from

"Three-Dimensional Simulation of Porosity in Plasma-Sprayed Alumina Using Microtomography and Electrochemical Impedance Spectrometry for Finite Element Modeling of Properties" by O. Amsellem, F. Borit, D. Jeulin, V. Guipont, M. Jeandin, E. Boller, and F. Pauchet

Abstract

Moving from a two-dimensional to a three-dimensional (3D) approach to microstructure and properties has been expected eagerly for a long while to result in a dramatic increase in the knowledge of thermally sprayed coatings. To meet these expectations, in the present study, microtomography and electrochemical impedance spectroscopy (EIS) were carried out to simulate the microstructure of plasma-sprayed alumina. As-sprayed and excimer laser-processed deposits were studied. Some unexpected but relevant results, e.g., regarding pore orientation in the coatings, could be obtained. EIS led to the establishment of an equivalent electrical circuit representation of the microstructure which enabled modeling of the insulating properties as a function of interfaces and pore interconnection. The pore interconnection was studied by microtomography. From this 3D simulation, a finite element analysis of Young's modulus properties was developed and compared to experiments. Using this approach, excimer laser surface processing was shown to be an innovative

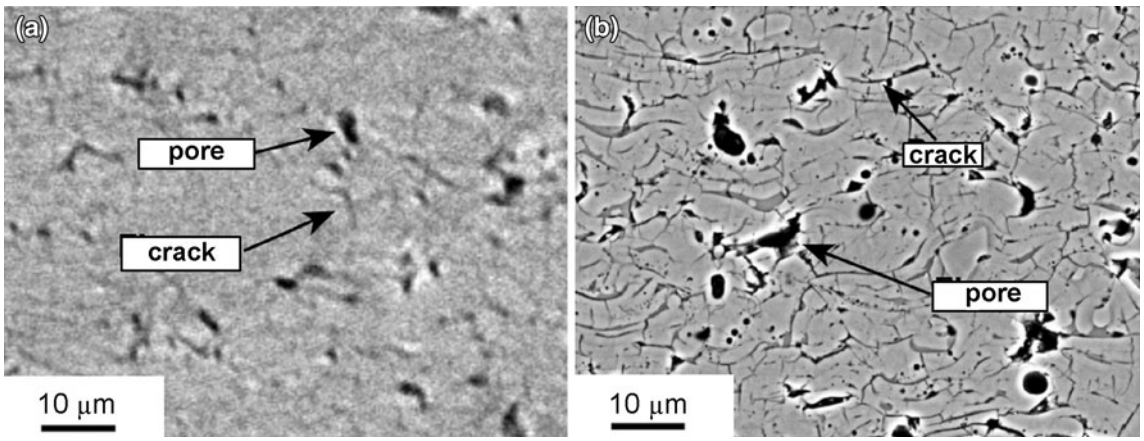

Fig. 2 (**a**) XMT and (**b**) SEM cross-sectional images of "A" alumina coating

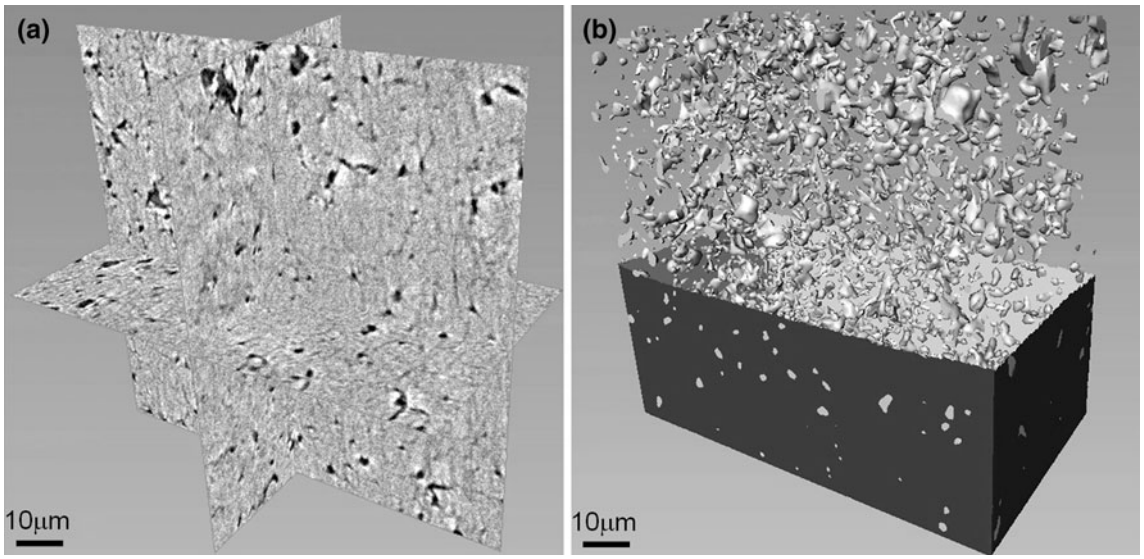

Fig. 3 3D porosity in $(56\ \mu m)^3$ "A" alumina coating volume, (**a**) XMT image and (**b**) IA-reconstructed

process to modify insulating characteristics of plasma-sprayed alumina.

Introduction

Alumina (Al_2O_3) is used extensively for its electrical insulating properties because of its high dielectric strength [1]. Thermal spraying, e.g., plasma spraying, is a prominent process for depositing low-cost high-performance dielectric coatings such as those made of pure alumina. Thermally sprayed alumina coatings show a composite microstructure because of the presence of defects, such as pores, inter-lamellar and intra-lamellar cracks, which can be considered as a second phase in an alumina matrix. These second phase features influence the mechanical behavior and electrical insulation of the coating dramatically [2, 3]. Several studies were published relating physical properties to plasma-sprayed coating microstructure [4–8]. The present study is based on the study of composite microstructures (according to the above mentioned definition, i.e., alumina + porosity) obtained by air plasma spraying (APS). Following an earlier 2-dimensional (2D) approaches to this issue [9, 10], a 3-dimensional (3D) approach is developed to relate pore and crack interconnection, which is difficult through 2D methods. Two 3D tools were used, first, microtomography [11], a dramatic development of which dates back to a few years ago only and, second, electrochemical impedance spectroscopy (EIS), the potential of which for correlating microstructure with coating properties was shown also recently [12, 13]. The 3D approach allows the determination of thermo-mechanical and electrical properties, e.g., primarily the Young's Modulus, which can be compared to those from the 2D approach [9, 10]. To demonstrate the advantages of the 3D approach, a new excimer laser process of coating was developed as a tool to explore the

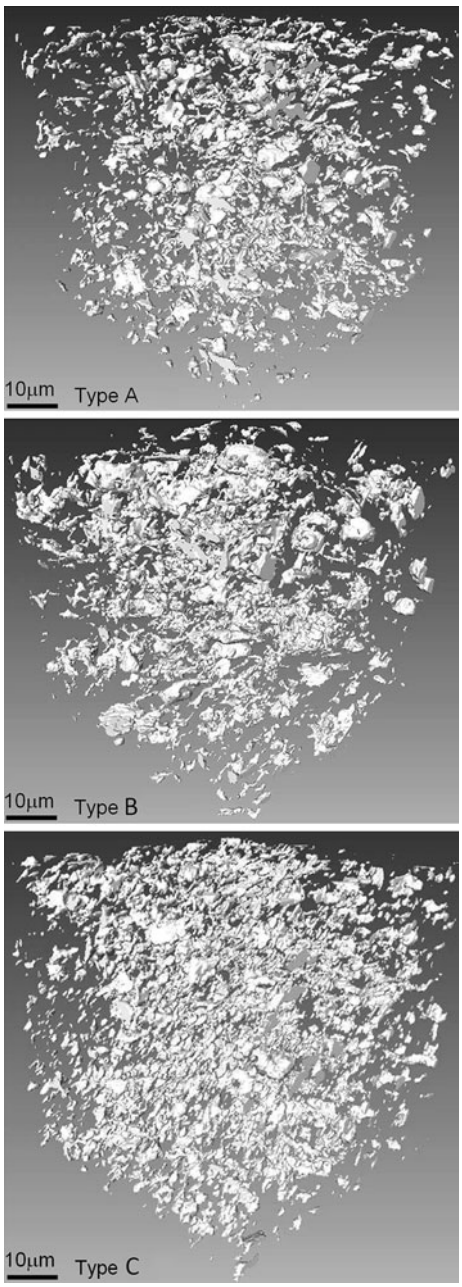

Fig. 4 XMT 3D images of a 70 × 70 × 70 μm^3 alumina volume for A, B, and C spraying conditions

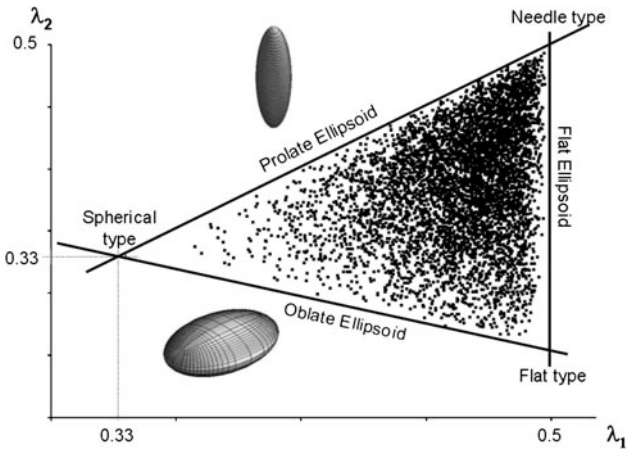

Fig. 8 Pore morphology in the [λ_1, λ_2] plane (e.g., A spraying conditions)

performance of the 3D approach. The process is new because conventional excimer laser processing is generally restricted to metals [14], rather than to ceramics, the study of which is relatively unexplored [15, 16].

Microstructure

2D tomographs, i.e., XMT images, compared well with scanning electron micrographs (SEM) (Fig. 2). Cracks and pores could be easily visualized on 2D tomographs. However, even though cracks could be detected in the XMT, they could not be exhibited in 3D-reconstructed images, because of a resolution which was limited to 0.6 μm^3 (Fig. 3). Further study, currently in progress, on image analysis (IA) using advanced gray level processing in particular, is required to resolve crack features. The absence of cracks in 3D images and the XMT resolution might explain the differences in the pore volume obtained from 2D, 3D image, and experimental analyses. 6 and 7.5% were measured, respectively, for 2D pore volume and 2D overall porosity, whereas 2.8% was calculated with XMT analysis for sample A (Fig. 4). Concerning equivalent spraying condition, 17.5% of porosity was measured experimentally [18]. In addition to conventional analyses, volume and volume density of pore (Fig. 8, 9), the so-called pore mass distribution was determined on the basis of an original study by Parra-Denis et al. [19]. Porosity size and distribution for the as-sprayed coatings could be exhibited nicely in 3D XMT images. Similar 3D analysis was applied to laser surface-processed "A" coating. When coupled to 2D SEM cross-sectional observation, 3D XMT showed superficial and inner cavities because of degassing in addition to pitting effects at the lowest laser energy density and glazing at upper densities (i.e., 4 and 8 J cm^{-2}).

For as-sprayed coatings, a mass-distribution parameter was used to study the pore morphology. The moments of inertia of a given object depend on its shape and characterize the distribution of mass within the shape. They correspond to the eigenvalue in the inertia matrix of the shape. The normalized moments are defined as $\lambda_i = I_i/(I_1 + I_2 + I_3)$, $i = 1, 2, 3$, where I_i are the moments of inertia. Their sum is equal to 1 s and they are ranked as $\lambda_1 > \lambda_2 > \lambda_3$. From those equations and the definition of

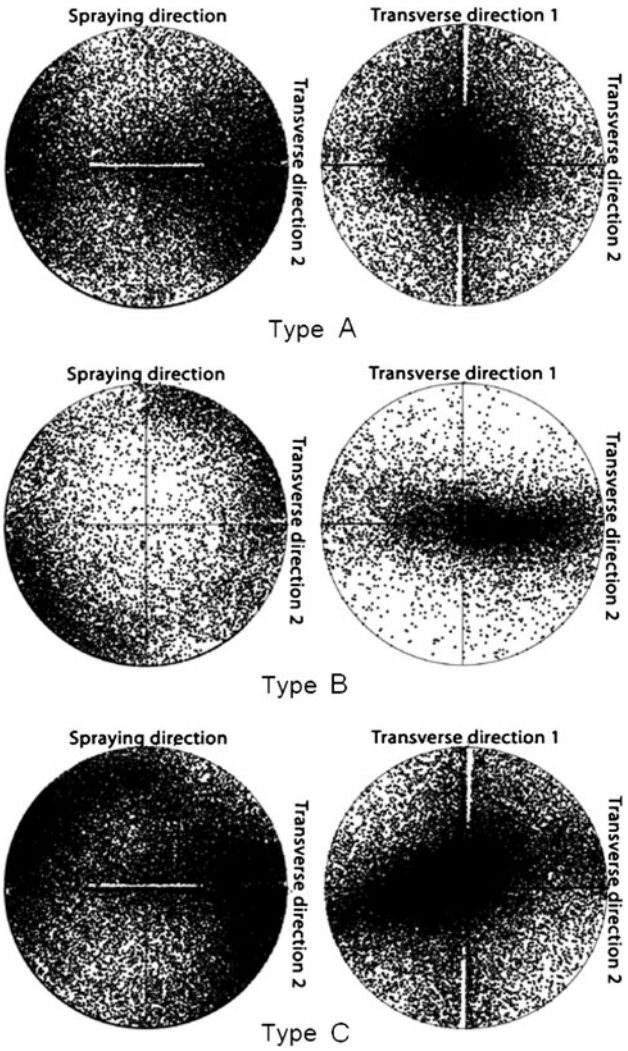

Fig. 9 Stereographic plot of the principal axis of inertia for pore orientation in A, B, and C

inertia moments, the two following expressions could be inferred: $\lambda_i \leq 0.5$ and $\lambda_2 \geq 0.5(1 - \lambda_1)$. These equations led to the 3D shape of pores in a 2D plane graph (Fig. 8).

Three types of mass distribution were exhibited: i.e., spherical, flat, and needle. Along the border lines, the shape was that of a prolate ellipsoid, an oblate ellipsoid, or a flat ellipsoid. The pores did not show a spherical shape. The mass distribution was similar to needle (Fig. 8). To know the orientation of the pores in the alumina material, a stereographic representation was used. The 2D stereographic plot of the principal axis of inertia for the whole particle (Fig. 9) showed that pores exhibited an orientation parallel to the spraying axis.

Three-Dimensional Modeling

The 3D images were adopted to define a finite element model. This consists in generating triangulated surface models using "Amira®" software [10, 20] and building an unstructured tetrahedral mesh based on this surface definition (Fig. 10). A characteristic of such meshing was to be highly dense, i.e., of 4 million nodes in a $(30\ \mu m)^3$ volume typically, which allowed to outline the pores precisely. 3D meshing was characterized by sub-domains in the calculated volume, which resulted from parallel calculations using Zebulon® (FEA program; Mines ParisTech, Centre des Materiaux). A tensile test was simulated to calculate the effective Young's modulus. Properties of alumina matrix was C1 = 310 GPa. Complexity of the matrix, i.e., the defect and the anisotropy behavior, were not characterized in this preliminary calculation. The effective Young's Modulus was determined from the expression:

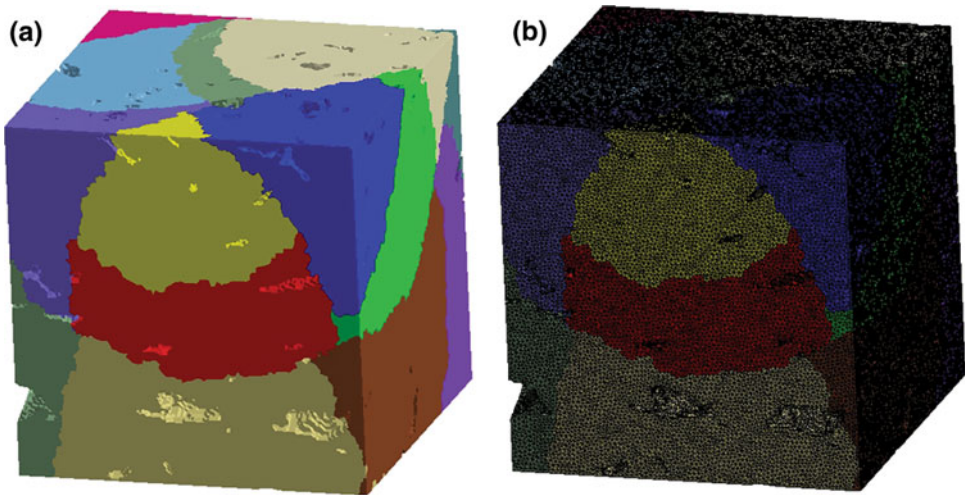

Fig. 10 (**a**) Sub-domain division, and (**b**) meshing of a calculated alumina volume

$$E_{\text{eff}} = \frac{V_{Al_2O_3}}{V}\frac{L(\sigma)}{\Delta L},$$

where $V_{Al_2O_3}$ is the volume of alumina, V is the total volume (porosity plus alumina matrix), ΔL is the prescribed displacement, L is the horizontal or vertical dimension in the model, and $\langle\sigma\rangle$ is the stress average calculated in the alumina material. Using the above-described meshing, Young's Modulus was determined to be equal to 260 GPa along the spraying direction. Calculations were made for a porosity of 3%, which is typically that of the studied materials (Type "C"). They showed the rather low influence of porosity on the elastic behavior. However, this calculated Young's Modulus was overestimated, as could be expected since cracks could not be involved in calculations. Another calculation error (±10 GPa) comes from the homogenization method of the finite element simulation. To add crack details, 3D images from microtomography should be improved for better IA in the reconstruction stage. Study is currently in progress to meet this objective. A typical value for the Young's Modulus should be then around 90 GPa as obtained experimentally with bending test method [21]. Further study should cover also a statistical study of the elementary volume for calculations to be significant actually.

Conclusion

Moving to the third dimension was shown to result in a dramatic improvement in the knowledge of the microstructure and properties of thermally sprayed coatings, e.g., alumina coatings in this study. Two major tools were developed for this. The first tool was XMT coupled with finite element analysis. In addition to the measurements of conventional porosity characteristics, the advanced processing of XMT 3D images allowed for studying the shape and the orientation of the pores. 3D analysis of microstructure has shown the complex morphology of pores which cannot be limited to ellipsoid in 2D observations. For sprayed alumina, the pores were seen to be oriented along the spraying direction although one could have expected a perpendicular orientation. The exploitation of XMT images could also feature the influence of excimer laser surface processing. This part showed the high sensitivity of the method since this fairly innovative laser treatment was shallow basically. The second tool consisted of EIS. EIS resulted in an experimental measurement of porosity (including cracks) interconnection in thermal spray microstructures through the definition of an electrical circuit equivalent to the involved pore-coating-substrate system. Further study remains to be done, mainly based on the achievement of better IA of XMT images to exhibit cracks and the improved definition of pores. From this development, one should expect to have at one's disposal a powerful enough tool to optimize excimer laser processing for the sealing of plasma-sprayed ceramic coatings such as alumina coatings.

References

1. R. Gadow, A. Killinger, A. Friedrich, A. Voss, Combined metallurgical and ceramic coating in the development of tubular ozone generators, in *Thermal Spray: Meeting the Challenges of the 21st Century*, ed. by C. Coddet, 25–29 May 1998 (Nice, France) (ASM International, Materials Park, OH, 1998), pp. 1083–1089
2. L. Pawlowski, The relationship between structure and dielectric properties in plasma sprayed alumina coating. Surf. Coat. Technol. **35**, 285–298 (1998)
3. S. Beauvais, V. Guipont, M. Jeandin, D. Juve, D. Treheux, A. Robisson, R. Saenger, Influence of defect orientation on electrical insulating properties of plasma-sprayed alumina coatings. J. Electroceram. **15**, 65–74 (2005)
4. C.J. Li, A. Ohmori, Relationships between the microstructure and properties of thermally sprayed deposits. J. Therm. Spray Technol. **11**, 365–374 (2002)
5. S. Beauvais, V. Guipont, E. Borit, M. Jeandin, M. Espanol, K.A. Khor, A. Robisson, R. Saenger, Process-microstructure-property relationships in controlled atmosphere plasma spraying (CAPS) of ceramics. Surf. Coat. Technol. **183**, 204–211 (2004)
6. O. Sarikaya, Effect of some parameters on microstructure and hardness of alumina coatings prepared by air plasma spraying. Surf. Coat. Technol. **190**, 388–393 (2005)
7. G. Bolelli, V. Cannillo, L. Lusvarghi, T. Manfredini, Glass–alumina composite coatings by plasma spraying. Part I: microstructural and mechanical characterization. Surf. Coat. Technol. **201**, 458–473 (2006)
8. Z. Wang, A. Kulkarni, S. Deshpande, T. Nakamura, H. Herman, Effects of pores and interfaces on effective properties of plasma sprayed zirconia coatings. Acta Mater. **51**, 5319–5334 (2003)
9. O. Amsellem, F. Borit, V. Guipont, M. Jeandin, F. Pauchet, A, Composite approach to Al_2O_3 based plasma sprayed coatings, in *Surface Modification Technologies*, ed. by T.S. Sudarshan, J.J. Stiglich. 25–29 Sept 2006 (Vienna) (ASM International, Materials Park, OH, 2007), pp. 30–34
10. O. Amsellem, K. Madi, F. Borit, D. Jeulin, V. Guipont, M. Jeandin, E. Boller, F. Pauchet, Two-dimensional (2D) and three-dimensional (3D) analyses of plasma-sprayed alumina microstructures for finite element simulation of Young's Modulus. J. Mater. Sci. **43**, 4091–4098 (2008)
11. F. Beckmann, R. Grupp, A. Haibel, M. Huppmann, M. Nothe, A. Pyzalla, W. Reimers, A. Schreyer, R. Zettler, In-situ synchrotron X-ray microtomography studies of microstructure and damage evolution in engineering materials. Adv. Eng. Mater. **9**, 939–950 (2007)
12. R. Saenger, D. Martin, C. Gabrielli, Electrochemical characterization of plasma sprayed WC-Co coatings by impedance techniques. Surf. Coat. Technol. **194**, 335–343 (2004)
13. C. Liu, An electrochemical impedance spectroscopy study of the corrosion behaviour of PVD coated steels in 0.5 N NaCl aqueous solution: part I. Establishment of equivalent circuits for EIS data modelling. Corros. Sci. **45**, 1243–1256 (2004)
14. G. Marest, Excimer laser processing of gray iron: microstructural and tribological characterization. Hyperfine Interact. **112**, 39 (1998)

15. Z. Liu, Crack-free surface sealing of plasma-sprayed ceramic coating using an excimer laser. Appl. Surf. Sci. **186**, 135–139 (2002)
16. A. Ibrahim, H. Salem, S. Sedky, Excimer laser surface treatment of plasma sprayed alumina–13% titania coatings. Surf. Coat. Technol. **203**, 3579–3589 (2009)
17. L. Salvo, P. Cloetens, E. Maire, S. Zabler, J.J. Blandin, J.Y. Buffiere, W. Ludwig, E. Boller, D. Bellet, C. Josserond, X-ray micro-tomography an attractive characterization technique in materials science. Nucl. Instrum. Methods Phys. Res. B **200**, 273–286 (2003)
18. S. Beauvais, V. Guipont, M. Jeandin, D. Jeulin, A. Robisson, R. Saenger, Study of the porosity in plasma-sprayed alumina through an innovative three-dimensional simulation of the coating buildup. Metall. Mater. Trans. A **39**, 2711–2724 (2008)
19. E. Parra-Denis, C. Barat, C. Ducottet, D. Jeulin, Three-D complex shape characterization by statistical analysis: application to aluminum alloys. Mater. Charact. **59**, 338–343 (2008)
20. K. Madi, S. Forest, M. Boussuge, S. Gailliègue, E. Lataste, J.Y. Buffière, D. Bernard, D. Jeulin, Finite element simulations of the deformation of fused-cast refractories based on X-ray computed tomography. Comput. Mater. Sci. **39**, 224–229 (2007)
21. J.H. You, T. Höschen, S. Lindig, Determination of elastic modulus and residual stress of plasma-sprayed tungsten coating on steel substrate. J. Nucl. Mater. **348**, 94–101 (2006)
22. J. Zhang, V. Desai, Evaluation of thickness, porosity and pore shape of plasma sprayed TBC by electrochemical impedance spectroscopy. Surf. Coat. Technol. **190**, 98–109 (2005)
23. B. Jayaraj, S. Vishweswaraiah, V.H. Desai, Y.H. Sohn, Electrochemical impedance spectroscopy of thermal barrier coatings as a function of isothermal and cyclic thermal exposure. Surf. Coat. Technol. **177–178**, 140–151 (2004)
24. C. Batista, A. Portinha, R.M. Ribeiro, V. Teixeira, M.F. Costa, C.R. Oliveira, Surface laser-glazing of plasma-sprayed thermal barrier coatings. Appl. Surf. Sci. **247**, 313–319 (2005)